Magnetic properties of X-C_2N (X=Cl, Br and I) monolayers: A first-principles study

Cite as: AIP Advances **8**, 055333 (2018); https://doi.org/10.1063/1.5025881
Submitted: 14 February 2018 . Accepted: 22 May 2018 . Published Online: 31 May 2018

Jingzhong Zhu, Muhammad Zulfiqar, Shuming Zeng, Yinchang Zhao, and Jun Ni

Magnetic properties of X-C_2N (X=Cl, Br and I) monolayers: A first-principles study

Jingzhong Zhu,[1,2] Muhammad Zulfiqar,[1,2] Shuming Zeng,[1,2] Yinchang Zhao,[3] and Jun Ni[1,2,a]

[1]*State Key Laboratory of Low-Dimensional Quantum Physics, Department of Physics, Tsinghua University, Beijing 100084, People's Republic of China*
[2]*Collaborative Innovation Center of Quantum Matter, Beijing 100084, People's Republic of China*
[3]*Department of Physics, Yantai University, Yantai 264005, People's Republic of China*

(Received 14 February 2018; accepted 22 May 2018; published online 31 May 2018)

The electronic and magnetic properties of X-C_2N (X=F, Cl, Br and I) monolayers have been systematically investigated from first-principles calculations. The F atom can be strongly adsorbed on the top of the host carbon atoms, while the Cl, Br and I atoms favor the top of the host nitrogen atoms of C_2N monolayers. These functionalized X-C_2N (X=F, Cl, Br and I) monolayers exhibit interesting electronic and magnetic features. The F-C_2N monolayer system shows a nonmagnetic metallic state, while the X-C_2N (X=Cl, Br and I) monolayer systems exhibit the magnetic semiconducting ground state. Moreover, the ferromagnetic state is energetically more stable configuration for the X-C_2N (X=Cl, Br and I) monolayer systems. Magnetic analysis further elaborates that the induced magnetism in the X-C_2N (X=Cl, Br and I) monolayer systems mainly arises from the local magnetic moments of the halogen adatoms. Thus, the chemical functionalization of nitrogenated honey graphene through halogen atoms adsorption has promising applications in electronic devices.
https://doi.org/10.1063/1.5025881

I. INTRODUCTION

Two-dimensional (2D) materials have been studied extensively by theoretical calculations and experiments since the discovery of graphene in 2004.[1–6] Many new 2D materials have been realized after graphene. Silicene, germanene and phosphorene have been synthesised on substrates.[7–12] In these 2D materials, graphene has a planar configuration without buckling height. By contrast, the silicene, germanene and phosphorene all show nonzero buckling height.[13–20] Besides the single-element 2D materials, compounds consisting of boron, carbon and nitrogen have intrigued much attention.[21–30] In particular, the C_2N monolayer has been realized in experiments.[31] The C_2N crystal was successfully synthesized by a simple wet chemical reaction.[31] The lattice structure of C_2N was confirmed with various characterization techniques, including scanning tunnelling microscopy.[31]

Since the successful synthesis of the C_2N monolayer, many applications of the C_2N monolayers have been proposed. Ca-embedded C_2N monolayer is a promising CO_2 adsorbent among the two dimensional materials.[32] The isovalent atom doped holey C_2N monolayers show interesting electronic characteristics and optical properties.[33] The Sc, Ti, V, Cr, Mn, Fe, Co and Ni atom-embedded C_2N monolayers induce a ferromagnetic ground state, while Cu atom-embedded C_2N monolayer possesses paramagnetic characteristics in the 2D C_2N monolayer.[34] In the meanwhile, the Zn atom-embedded C_2N monolayer exhibits a nonmagnetic ground state.[34] The zigzag C_2N nanoribbons with edge modifications have been proposed to be multi-functional spin devices.[35]

[a]Electronic mail: junni@mail.tsinghua.edu.cn

The C_2N crystal shows a finite band-gap of approximately 1.96 eV in experiments.[31] Especially, the highest valence bands of the C_2N monolayer are quasi-flat and the density of states (DOS) of the C_2N monolayer shows a van Hove singularity near the valence band maximum (VBM).[32–42] Van Hove singularities in a 2D material may lead to phase transitions such as ferromagnetism and superconductivity.[43–45] We have already reported such type of ferromagnetic half metallic phase transition with the help of hole doping in the pristine C_2N monolayer system from the first-principles calculations.[45] Furthermore, electron doping has also proved as an effective way to induce significant magnetism in the pristine C_2N monolayer.[43–45] Thus, it is important to study the chemical adsorption of halogen adatoms on the C_2N monolayer because the halogen atoms are highly prone to accepting electrons to further increase their stability.

In this paper, we have systematically investigated the electronic and magnetic properties of the X-C_2N (X=F, Cl, Br and I) monolayers by utilizing first-principles calculations. We find that the Cl, Br, and I adatoms can be strongly adsorbed on the top of the host nitrogen atoms, while the F atoms favor the top of the host carbon atoms of the C_2N monolayer. The F-C_2N monolayer system shows a nonmagnetic metallic state, while the chemically functionalized X-C_2N (X=Cl, Br and I) monolayer systems exhibit the magnetic semiconducting ground state with the ferromagnetic state being more energetically stable. Additionally, the magnetic analysis reveals the origin of such induced magnetism in the X-C_2N (X=Cl, Br and I) monolayer systems, which mainly arises from the local magnetic moments of the halogen adatoms.

The outline of this paper is as follows: Section II describes the calculation methods. In Sec. III, we show the structures of X-C_2N (X=F, Cl, Br and I) monolayers and discuss the electronic and magnetic properties of the system. Section IV is the summary.

II. METHODS

We have performed spin-polarized density functional theory (DFT) calculations implemented in the Vienna ab initio simulation package (VASP).[46,47] We have adopted the projector-augmented wave (PAW) potentials to model the core electrons, while to model the valance electrons a plane wave basis set with an energy cutoff of 500 eV is adopted. For exchange and correlation, we have utilized the generalized gradient approximation (GGA) of Perdew, Burke, and Ernzernhof (PBE).[48] A (2×2) C_2N supercell including 72 nonmetal atoms and an adsorbed halogen atom is employed. The vacuum region between adjacent C_2N layers is kept larger than 15 Å to avoid images interactions. The Brillouin zone (BZ) sampling is obtained using a $6 \times 6 \times 1$ Monkhorst-Pack grid for relaxation calculations while a $12 \times 12 \times 1$ Monkhorst-Pack grid is adopted for the static calculations.[49] The tolerance of the energy convergence is set to 10^{-5} eV. We have relaxed all the structures until the forces on each atom become smaller than 0.01 eV/Å.

III. RESULTS AND DISCUSSIONS

The lattice structure of the pristine C_2N monolayer is shown in Fig. 1. We give the top view and side view of a 2×2 supercell of the pristine C_2N monolayer. A primitive cell of the pristine C_2N monolayer contains twelve carbon (C) atoms and six nitrogen (N) atoms, as depicted in Fig. 1(a). The pristine C_2N monolayer possesses planar configuration without any buckling. The lattice constant of the pristine C_2N monolayer is 8.328Å, which agrees well with the experiment measurement and previous theoretical studies.[31,43–45] The B_1 and B_2 C-C bond lengths are 1.470Å and 1.430Å, respectively. The B_3 C-N bond length is 1.336Å. The structure of the pristine C_2N monolayer can be considered as carbon rings further connected by nitrogen atoms.

We have considered adsorption of a single halogen atom on the 2×2 supercell of the C_2N monolayer. One side adsorption of nanosheet may induce curved structure.[50–52] In our case, the coverage of adsorption atoms is about 1.4%, which is small and the effect of the adsorption induced stress will be weak. Eight possible adsorption sites are chosen on the C_2N monolayer i.e. three hollow sites (H_1, H_2 and H_3), three bridge sites (B_1, B_2 and B_3), and two top sites (T_1 and T_2). More precisely, H_1 represents the largest hollow sites of the C_2N monolayer, whereas H_2 and H_3 denote the hollow sites of the C-N rings and the C-C rings of the C_2N monolayer, respectively. Furthermore,

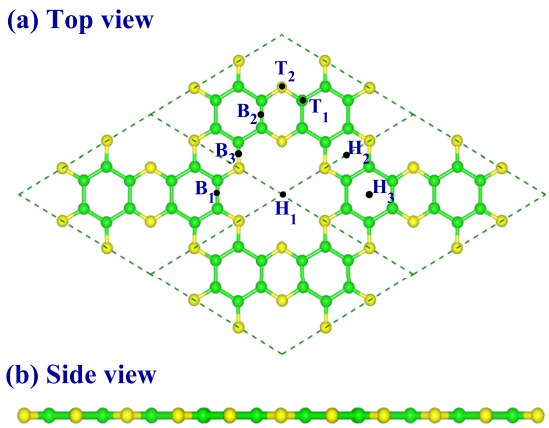

FIG. 1. The lattice structure of the pristine C_2N monolayer. (a) Top view. (b) Side view. H_1, H_2 and H_3 denotes the three hollow sites of the C_2N monolayer. B_1, B_2 and B_3 denotes the corresponding three bridge sites of the C_2N monolayer. T_1 and T_2 denotes the two top sites of the C_2N monolayer. The green and yellow balls represent carbon and nitrogen atoms, respectively.

B_1 and B_2 represent two different C-C bridge sites whereas B_3 represents the C-N bridge sites. Similarly, T_1 and T_2 denote the top sites of the carbon and nitrogen atoms, respectively.

The most stable adsorption site identified for the Cl-C_2N, Br-C_2N and I-C_2N monolayer systems is the T_2 site which represents the atop site of the host nitrogen atoms of the C_2N monolayer. The optimized structures of X-C_2N (X=Cl, Br and I) monolayers with the adsorbed halogen atoms on their most stable adsorption sites are presented in Fig. 2 with Cl-C_2N as an example. The binding energy is defined as $E = E_d - E_0 - E_m$, where E_d and E_0 are the energies with and without the adsorbed halogen atoms, respectively. Whereas E_m is the energy of a free halogen atom. The binding energy of Cl-C_2N, Br-C_2N and I-C_2N with the halogen atoms on the most stable adsorption sites T_2 are 446 meV, 275 meV and 177 meV, respectively. In the eight adsorption sites we have considered, the B_3 site can be regarded as the most unique unstable adsorption site. Because all the halogen atoms likely to be reside on the T_1 sites after structure relaxation, which may comes from the symmetry issue because the B_3 site is one of the most unique unsymmetrical site in the eight adsorption sites chosen.

The properties of the C_2N monolayers with the adsorbed halogen atoms in their most stable adsorption sites are listed in Table I. The lattice constants of the X-C_2N (X=F, Cl, Br and I) monolayers are about 16.656Å. Because we have choose a 2×2 supercell to calculate the electronic and magnetic

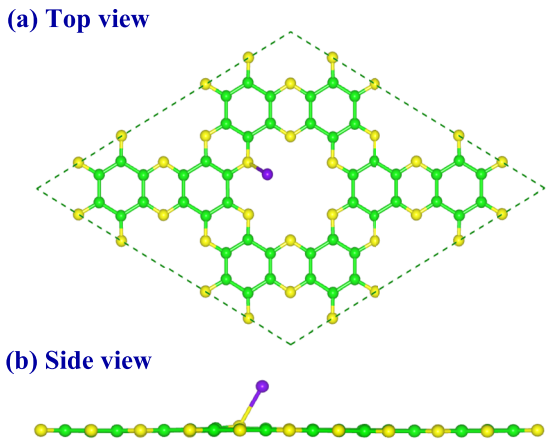

FIG. 2. The optimized structure of Cl-C_2N with Cl atoms in the most stable adsorption sites. (a) Top view. (b) Side view. The green and yellow balls represent carbon and nitrogen atoms, respectively. The purple balls represent the Cl atoms.

TABLE I. The lattice constant (a), the height from the halogen atom to the C_2N plane (h), the angle between the X-N (X=Cl, Br and I) bond (or F-C bond) and the C_2N plane (θ), the nearest C-N bond length (l_{C-N}) of the halogen atom, the X-N (X=Cl, Br and I) bond (or F-C bond) length (l), the band gap (E_g) and the total magnetic moment of the system (μ_{tot}).

	a (Å)	h (Å)	θ (∘)	l_{C-N} (Å)	l (Å)	E_g (eV)	μ_{tot} (μ_B)
C_2N	16.656	...	...	1.336	...	1.670	...
F-C_2N	16.657	2.059	90.000	1.418	1.468	0.000	0.000
Cl-C_2N	16.656	2.223	60.058	1.337	2.395	0.825	1.000
Br-C_2N	16.655	2.389	59.393	1.337	2.605	0.629	1.000
I-C_2N	16.656	2.404	51.394	1.337	2.969	0.398	1.000

properties of the X-C_2N (X=F, Cl, Br and I) monolayers, thus the lattice constants of the X-C_2N (X=F, Cl, Br and I) monolayers are about 2 times of the lattice constant (8.328Å) of the primitive cell of the C_2N monolayer. The conclusions can be made from the lattice constants calculations of the X-C_2N (X=F, Cl, Br and I) monolayers which are as follows: (1) The lattice constants of X-C_2N (X=F, Cl, Br and I) monolayers are entirely insensitive to the kind of the adsorb halogen atoms. (2) The X-C_2N (X=F, Cl, Br and I) monolayers are stable.

The optimize heights obtained from the adsorbed halogen atoms (F, Cl, Br and I) and the C_2N monolayer plane are 2.059Å, 2.223Å, 2.389Å and 2.404Å, respectively. Although the most stable adsorption sites for the corresponding adsorbed halogen atoms (Cl, Br and I) are all T_2, the projection positions of these three types of halogen atoms on the C_2N plane are not the positions of the nitrogen atoms. To depict the departure of these three types of halogen atoms from the rigorous T_2 sites, we define an angle (θ) which is the angle between the X-N (X=Cl, Br and I) bond and the C_2N plane. The θ for Cl, Br and I are 60.058°, 59.393° and 51.394°, respectively. The θ for F means the angle is 90.000° between the F-C bond and the C_2N plane. The C-N bond lengths are 1.337Å for Cl-C_2N, Br-C_2N and I-C_2N, which demonstrates again the stability of the C_2N monolayer after the adsorption of the halogen atoms. The X-N bond lengths for Cl, Br and I are 2.395Å, 2.605Å and 2.969Å, respectively. The difference of the X-N (X=Cl, Br and I) bond lengths arises partially from the different radius of the halogen atoms.

The electronic band structures of the pristine C_2N, the Cl-C_2N, the Br-C_2N and the I-C_2N monolayer systems are shown in Figs. 3(a)–3(d). The electronic band structures of the F-C_2N are shown at last as its properties are different from those of the X-C_2N (X=Cl, Br and I) monolayers. The band gap of the C_2N monolayer is 1.670eV, which agrees well with the previous calculations.[43–45] The band gap is smaller than the experiment result (1.96eV),[31] which may come from the use of the PBE exchange and correlation functional because the PBE usually underestimates the band gaps

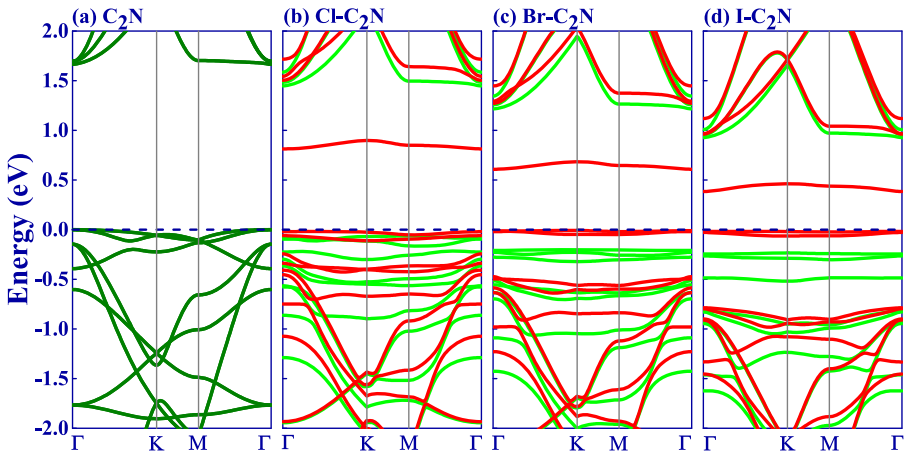

FIG. 3. The electronic band structures of (a) the pristine C_2N (b) Cl-C_2N (c) Br-C_2N and (d) I-C_2N monolayers, respectively. The green and red solid lines represent the spin-up and spin-down electronic bands, respectively.

of the semiconductors and insulators. The valence band maximum (VBM) and the conduction band minimum (CBM) locate at the Γ point. Some flat electronic bands emerge near the VBM and a sharp van Hove singularity emerges in the density of states of the C_2N monolayer. Since the van Hove singularity of the pristine C_2N monolayer locates near the VBM, we can tailor the electronic and magnetic features of the C_2N monolayer by utilizing the available van Hove singularity. The hole-doped C_2N monolayers show half metallic nature with ferromagnetic ground state whereas the electron-doping in the C_2N monolayer induce significant magnetic moments.[43–45] Since the halogen atoms are highly prone to accepting electrons to increase their stability, thus we expect significant modification in the electronic and magnetic behaviors of the functionalized structures, which are further confirmed from the spin polarized band structures of the Cl-C_2N, the Br-C_2N and the I-C_2N monolayer systems.

The calculated bandgaps of the Cl-C_2N, the Br-C_2N and the I-C_2N monolayer systems are 0.825eV, 0.629eV and 0.398eV, respectively. The bandgaps of the X-C_2N (X=Cl, Br and I) monolayers are smaller than the bandgap (1.670eV) of the pristine C_2N monolayer. Strikingly, some flat subbands emerge near the Fermi level in the the Cl-C_2N, Br-C_2N and I-C_2N monolayer systems. It can also be noticed that the highest valence band and the lowest conduction band of the X-C_2N (X=Cl, Br and I) monolayers are fully spin polarized, which suggests that all the conduction electrons available in the spin-down channel can be utilized at room temperature. The calculated net magnetic moment induced in the Cl-C_2N, the Br-C_2N and the I-C_2N monolayer systems is $1.000\mu_B$. Moreover, it can also be noticed from the spin polarized electronic band structures provided in the Figs. 3(c) and 3(d) which means the X-C_2N (X=Cl, Br and I) monolayers are magnetic semiconductors. Conventionally, in the common diluted magnetic semiconductors, the magnetism often originates from the doping of transition metal atoms.[53–55] It is important to notice that in the Cl-C_2N, the Br-C_2N and the I-C_2N monolayer systems, the magnetism originate from the halogen atoms.

We have also shown the distribution of charge density of spin-up state minus spin-down state of the X-C_2N (X=Cl, Br and I) monolayers in Fig. 4. The ferromagnet of the X-C_2N (X=Cl, Br and I) monolayers is localized on the halogen atoms. Halogen atoms are extensively utilized to tailor the electronic and magnetic properties of the 2D materials.[56–60] Additionally, it is reported that fluorination can successfully induce half-metallicity in the zigzag boron nitride nanoribbons or zinc oxide layers.[56,57] Thus the underlying magnetism mechanism in these proposed materials (Cl-C_2N, Br-C_2N and I-C_2N monolayers) is similar to those of Refs. 56–60.

To understand the magnetism of the X-C_2N (X=Cl, Br and I) monolayers from another perspective, the density of states (DOS) and the projected density of states (PDOS) of the Cl-C_2N and Br-C_2N are plotted in Fig. 5. Considering the similarity of the electronic band structures of the Br-C_2N and I-C_2N monolayer systems, we take the DOS and PDOS of the Br-C_2N as an example to explore the magnetism. The C and N atoms in Fig. 5 represent the nearest C atom and the nearest N atom of the corresponding halogen atom. The Cl-C_2N and Br-C_2N possess band gaps of 0.825eV and 0.629eV,

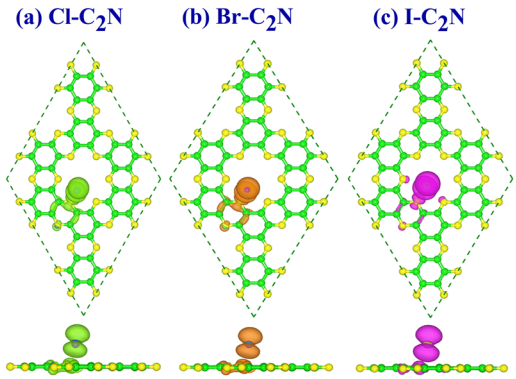

FIG. 4. Distribution of charge density of spin-up state minus spin-down state for (a) the Cl-C_2N (b) the Br-C_2N and (c) the I-C_2N, respectively. The isosurface value is taken to be 0.002 $e\AA^{-3}$. The green, the orange and the purple colors label the spin-up charges of the Cl-C_2N, the Br-C_2N and the I-C_2N monolayer systems, respectively.

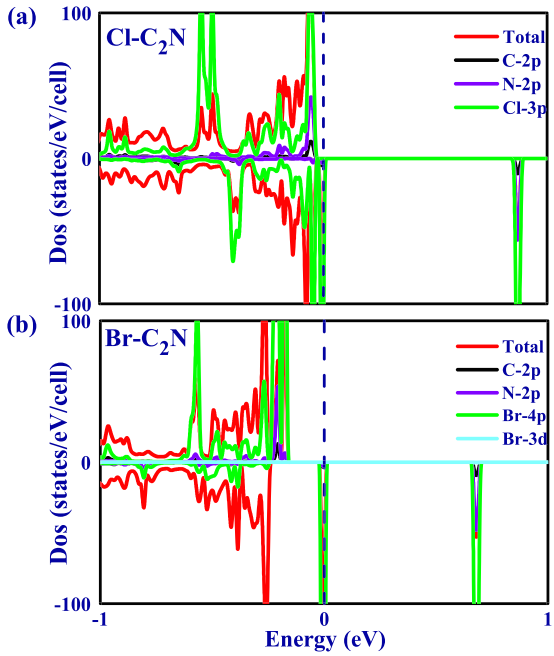

FIG. 5. The total and orbital resolved DOS for (a) Cl-C_2N and (b) Br-C_2N. The C atom and N atom represent the nearest C atom and the nearest N atom of the corresponding halogen atom. All the PDOSs are magnified by 10 times.

respectively, which agrees well with the electronic band structures in Fig. 3. The peaks of the DOS near the VBM and CBM in Fig. 5 have a good correspondence with the flat sub-bands in Fig. 3. Figures 5(a) and 5(b) shows that the hybridized *p*-orbitals of dopants and *p*-orbitals of the nearest C and N atoms mainly contribute to the induced impurity states. The peaks near the Fermi level of the DOS of the Cl-C_2N and Br-C_2N come mostly from the *p* orbitals of the N atoms and the halogen atoms. A strong hybridization emerges between the *p* orbitals of the N atom and the *p* orbitals of the halogen atoms. The p-p hybridization leads to the split of the energy level near the Fermi energy, the split from the p-p hybridization is the origin of the induced magnetism in the X-C_2N (X=Cl, Br and I) monolayers.

In order to explore the magnetic ground state of the X-C_2N (X=Cl, Br and I) monolayers, an antiferromagnetic (AFM) configuration has been considered in Fig. 6. Our calculations indicate that the local magnetic moment of the X-C_2N (X=Cl, Br and I) monolayers is insensitive with the size of the supercell. One X atom (X=Cl, Br and I) induces 1.000μ_B local magnetic moment for (1×1), (1×2) or (2×2) X-C_2N (X=Cl, Br and I) supercells. The geometry, the energy for the ferromagnetic (FM), AFM, nonmagnetic (NM) configuration have been calculated for the X-C_2N (X=Cl, Br and I) monolayers. We set the energy of FM of the X-C_2N (X=Cl, Br and I) monolayers as 0. The energy of AFM of the X-C_2N (X=Cl, Br and I) monolayers are calculated to be 1.03meV, 0.65meV and 0.22meV, respectively. The energy of NM of the X-C_2N (X=Cl, Br and I) monolayers are 1.006eV, 0.951eV and 0.959eV, respectively. The ferromagnetic state is the most energetically stable configuration for the X-C_2N (X=Cl, Br and I) monolayers. The corresponding magnetic moment for a (2×2) X-C_2N (X=Cl, Br and I) supercell is 4.000 μ_B for the FM state.

At last, we give the optimized structure and electronic structure of F-C_2N with the F atom in the most stable adsorption site in Fig. 7. The most stable adsorption site of the F atom is the top site of the C atom in the C_2N monolayer, which is different from the most stable adsorption sites of Cl, Br and I atoms. The F-C bond length is 1.468Å and the height from the F atom to the C_2N plane is 2.059Å. Figure 7(b) shows that a small distortion occurs when the F atoms adsorbed on the top site of the C atom. The height from the nearest C atom of the F atom to the C_2N plane is 0.602Å. The F-C_2N exhibits metallic feature as the Fermi level cross with an impurity band, as illustrated in Fig. 7(c), which is different from the semiconductor features of the X-C_2N (X=Cl, Br and I) monolayers. The F-C_2N exhibits nonmagnetic characteristics with the symmetry of the DOS

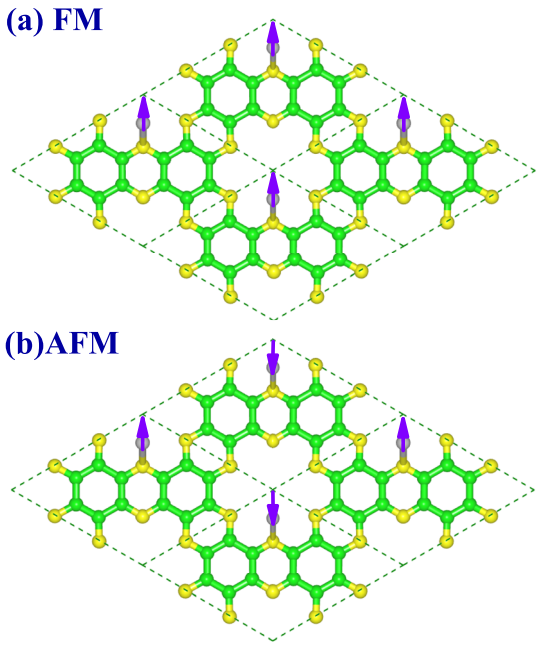

FIG. 6. The optimized configurations, local magnetic arrangements for (a) FM and (b) AFM. The green, the yellow and the gray balls represent the C, the N and the Cl atoms, respectively.

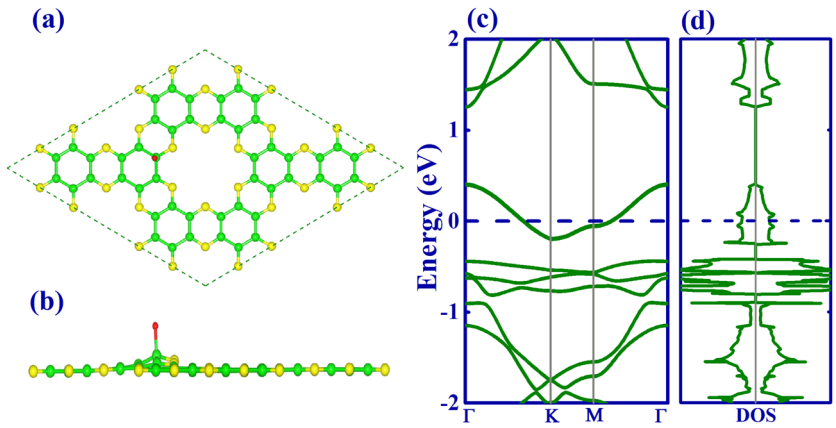

FIG. 7. The optimized structure and electronic structure of F-C_2N with F atoms on the most stable adsorption site. (a) Top view. (b) Side view. (c) Electronic band. (d) Density of states (DOS). The green, the yellow and the red balls represent the C, the N and the F atoms, respectively.

in Fig. 7(d), which is different from the ferromagnetic ground states of the X-C_2N (X=Cl, Br and I) monolayers. The adsorption site, the electronic and magnetic properties of F-C_2N are different from that of the X-C_2N (X=Cl, Br and I) monolayers.

IV. CONCLUSION

We have studied the electronic and magnetic features of the X-C_2N (X=F, Cl, Br and I) monolayers from first-principles calculations. The F atom can be strongly adsorbed on top of the host carbon atoms, while the Cl, Br and I atoms favor top of the host nitrogen atoms of C_2N monolayers. The F-C_2N monolayer system shows a nonmagnetic metallic state, while the Cl-C_2N, the Br-C_2N and the

I-C_2N monolayers exhibit a net magnetic moment of 1.000μ_B. Moreover, the ferromagnetic state is energetically most stable configuration for the X-C_2N (X=Cl, Br and I) monolayers. The spatial spin charge density distributions further demonstrate that the induced magnetism in the X-C_2N (X=Cl, Br and I) monolayers originates from the adsorbed halogen atoms. The Cl-C_2N, the Br-C_2N and the I-C_2N monolayer systems show different bandgaps in the electronic band structures. The electronic subbands near the Fermi energy of the X-C_2N (X=Cl, Br and I) monolayers are fully spin polarized. Functionalization of the C_2N monolayer through these halogen-atoms adsorption appears to be a promising way to extend its applications.

ACKNOWLEDGMENTS

This research was supported by the National Natural Science Foundation of China under Grant Nos. 11774195 and 11704322, the National Key Research and Development Program of China under Grant No. 2016YFB0700102, National S&T Major Project of China under Grant No. 2008ZX06901 and the Natural Science Foundation of Shandong Province for Doctoral Program under Grant No. ZR2017BA017.

[1] K. S. Novoselov, A. K. Geim, S. V. Morozov, D. Jiang, Y. Zhang, S. V. Dubonos, I. V. Grigorieva, and A. A. Firsov, Science **306**, 666 (2004).
[2] A. H. Castro Neto, F. Guinea, N. M. R. Peres, K. S. Novoselov, and A. K. Geim, Rev. Mod. Phys. **81**, 109 (2009).
[3] A. C. Ferrari, J. C. Meyer, V. Scardaci, C. Casiraghi, M. Lazzeri, F. Mauri, S. Piscanec, D. Jiang, K. S. Novoselov, S. Roth, and A. K. Geim, Phys. Rev. Lett. **97**, 187401 (2006).
[4] M. Y. Han, B. Ozyilmaz, Y. Zhang, and P. Kim, Phys. Rev. Lett. **98**, 206805 (2007).
[5] C. L. Kane and E. J. Mele, Phys. Rev. Lett. **95**, 226801 (2005).
[6] Y.-W. Son, M. L. Cohen, and S. G. Louie, Phys. Rev. Lett. **97**, 216803 (2006).
[7] W. Li, S. Sheng, J. Chen, P. Cheng, L. Chen, and K. Wu, Phys. Rev. B **93**, 155410 (2016).
[8] J. Qiu, H. Fu, Y. Xu, A. I. Oreshkin, T. Shao, H. Li, S. Meng, L. Chen, and K. Wu, Phys. Rev. Lett. **114**, 126101 (2015).
[9] M. Xu, T. Liang, M. Shi, and H. Chen, Chem. Rev. **113**, 3766 (2013).
[10] L. Zhang, P. Bampoulis, A. N. Rudenko, Q. Yao, A. van Houselt, B. Poelsema, M. I. Katsnelson, and H. J. W. Zandvliet, Phys. Rev. Lett. **116**, 256804 (2016).
[11] N. Ehlen, B. V. Senkovskiy, A. V. Fedorov, A. Perucchi, P. Di Pietro, A. Sanna, G. Profeta, L. Petaccia, and A. Gruneis, Phys. Rev. B **94**, 245410 (2016).
[12] K. J. Koski and Y. Cui, ACS Nano **7**, 3739 (2013).
[13] S. Z. Butler, ACS Nano **7**, 2898 (2013).
[14] X. Lin and J. Ni, Phys. Rev. B **86**, 075440 (2012).
[15] Y. Ge, W. Wan, F. Yang, and Y. Yao, New J. Phys. **17**, 035008 (2015).
[16] H. Pan, Z. Li, C.-C. Liu, G. Zhu, Z. Qiao, and Y. Yao, Phys. Rev. Lett. **112**, 106802 (2014).
[17] J. E. Padilha and R. B. Pontes, J. Phys. Chem. C **119**, 3818 (2015).
[18] V. Tran, R. Soklaski, Y. Liang, and L. Yang, Phys. Rev. B **89**, 235319 (2014).
[19] A. Ziletti, A. Carvalho, D. K. Campbell, D. F. Coker, and A. H. Castro Neto, Phys. Rev. Lett. **114**, 046801 (2015).
[20] X. Peng, Q. Wei, and A. Copple, Phys. Rev. B **90**, 085402 (2014).
[21] K. M. Krishnan, Appl. Phys. Lett. **58**, 1857 (1991).
[22] H. Yanagisawa, T. Tanaka, Y. Ishida, E. Rokuta, S. Otani, and C. Oshima, Phys. Rev. B **73**, 045412 (2006).
[23] Z. Weng-Sieh, K. Cherrey, N. G. Chopra, X. Blase, Y. Miyamoto, A. Rubio, M. L. Cohen, S. G. Louie, A. Zettl, and R. Gronsky, Phys. Rev. B **51**, 11229 (1995).
[24] A. Ueno, T. Fujita, M. Matsue, H. Yanagisawa, C. Oshima, F. Patthey, H.-C. Ploigt, W.-D. Schneider, and S. Otani, Surf. Sci. **600**, 3518 (2006).
[25] A. Du, S. Sanvito, and S. C. Smith, Phys. Rev. Lett. **108**, 197207 (2012).
[26] X.-F. Zhou, J. Sun, Y.-X. Fan, J. Chen, H.-T. Wang, X. Guo, J. He, and Y. Tian, Phys. Rev. B **76**, 100101 (2007).
[27] X. Luo, X. Guo, B. Xu, Q. Wu, Q. Hu, Z. Liu, J. He, D. Yu, Y. Tian, and H.-T. Wang, Phys. Rev. B **76**, 094103 (2007).
[28] X. Luo, X. Guo, Z. Liu, J. He, D. Yu, B. Xu, Y. Tian, and H.-T. Wang, Phys. Rev. B **76**, 092107 (2007).
[29] Q. Li, M. Wang, A. R. Oganov, T. Cui, Y. Ma, and G. Zou, J. Appl. Phys. **105**, 053514 (2009).
[30] Q. Hu, Q. Wu, Y. Ma, L. Zhang, Z. Liu, J. He, H. Sun, H.-T. Wang, and Y. Tian, Phys. Rev. B **73**, 214116 (2006).
[31] J. Mahmood, E. K. Lee, M. Jung, D. Shin, I.-Y. Jeon, S.-M. Jung, H.-J. Choi, J.-M. Seo, S.-Y. Bae, S.-D. Sohn, N. Park, J. H. Oh, H.-J. Shin, and J.-B. Baek, Nat. Commun. **6**, 6486 (2015).
[32] Y. Liu, Z. Meng, X. Guo, G. Xu, D. Rao, Y. Wang, K. Deng, and R. Lu, Phys. Chem. Chem. Phys. **19**, 28323 (2017).
[33] J. Du, C. Xia, T. Wang, W. Xiong, and J. Li, J. Mater. Chem. C **4**, 9294 (2016).
[34] J. Du, C. Xia, W. Xiong, X. Zhao, T. Wang, and Y. Jia, Phys. Chem. Chem. Phys. **18**, 22678 (2016).
[35] X. Yang, Y. Kuang, H. Yu, Z. Shao, J. Zhang, J. Feng, X. Chen, and Y. Liu, Phys. Chem. Chem. Phys. **19**, 12538 (2017).
[36] B. Xu, H. Xiang, Q. Wei, J. Q. Liu, Y. D. Xia, J. Yin, and Z. G. Liu, Phys. Chem. Chem. Phys. **17**, 15115 (2015).
[37] S. Chakrabarty, T. Das, P. Banerjee, R. Thapa, and G. P. Das, Appl. Surf. Sci. **418**, 92 (2017).
[38] J. Sun, R. Zhang, X. Li, and J. Yang, Appl. Phys. Lett. **109**, 133108 (2016).
[39] L. Zhu, Q. Xue, X. Li, T. Wu, Y. Jin, and W. Xing, J. Mater. Chem. A **3**, 21351 (2015).
[40] D. W. Ma, Q. Wang, X. Yan, X. Zhang, C. He, D. Zhou, Y. Tang, Z. Lu, and Z. Yang, Carbon **105**, 463 (2016).

[41] M. R. Ashwin Kishore and P. Ravindran, J. Phys. Chem. C **121**, 22216 (2017).
[42] Z. Hu, B. Liu, M. Dahanayaka, A. W.-K. Law, J. Wei, and K. Zhou, Phys. Chem. Chem. Phys. **19**, 15973 (2017).
[43] Z. Liang, B. Xu, H. Xiang, Y. Xia, J. Yin, and Z. Liu, RSC Adv. **6**, 54027 (2016).
[44] S. Gong, W. Wan, S. Guan, B. Tai, C. Liu, B. Fu, S. A. Yang, and Y. Yao, J. Mater. Chem. C **5**, 8424 (2017).
[45] J. Zhu, Y. Zhao, S. Zeng, and J. Ni, Phys. Lett. A **381**, 1097 (2017).
[46] G. Kresse and J. Furthmuller, Comput. Mater. Sci. **6**, 15 (1996).
[47] G. Kresse and J. Furthmuller, Phys. Rev. B **54**, 11169 (1996).
[48] G. Kresse and D. Joubert, Phys. Rev. B **59**, 1758 (1999).
[49] H. J. Monkhorst and J. D. Pack, Phys. Rev. B **13**, 5188 (1976).
[50] D. Yu and F. Liu, "Synthesis of carbon nanotubes by rolling up patterned graphene nanoribbons using selective atomic adsorption," Nano Lett. **7**, 3046–3050 (2007).
[51] J. Zang, M. Huang, and F. Liu, "Mechanism for nanotube formation from self-bending nanofilms driven by atomic-scale surface-stress imbalance," Phys. Rev. Lett. **98**, 146102 (2007).
[52] O. G. Schmidt and K. Eberl, "Nanotechnology: Thin solid films roll up into nanotubes," Nature **410**, 168 (2001).
[53] L. Bergqvist, O. Eriksson, J. Kudrnovsky, V. Drchal, P. Korzhavyi, and I. Turek, Phys. Rev. Lett. **93**, 137202 (2004).
[54] S.-R. E. Yang and A. H. MacDonald, Phys. Rev. B **67**, 155202 (2003).
[55] J. Konig, H.-H. Lin, and A. H. MacDonald, Phys. Rev. Lett. **84**, 5628 (2000).
[56] F. Zheng, G. Zhou, Z. Liu, J. Wu, W. Duan, B.-L. Gu, and S. B. Zhang, Phys. Rev. B **78**, 205415 (2008).
[57] Y. Wang, Y. Ding, and J. Ni, Phys. Rev. B **81**, 193407 (2010).
[58] Q. Chen, J. Wang, L. Zhu, S. Wang, and F. Ding, J. Chem. Phys. **132**, 204703 (2010).
[59] Q. Chen, L. Zhu, and J. Wang, Appl. Phys. Lett. **95**, 133116 (2009).
[60] A. R. Botello-Mendez, F. Lopez-Urias, M. Terrones, and H. Terrones, Nano Lett. **8**, 1562 (2008).